Analyst

Accepted Manuscript

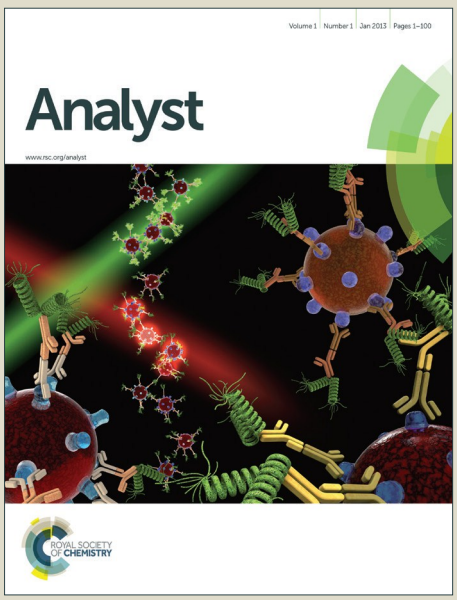

ROYAL SOCIETY OF CHEMISTRY

www.rsc.org/analyst

Analyst

Revised; 27 September 2015

Top-Down Mass Spectrometry of Hybrid Materials with Hydrophobic Peptide and Hydrophilic or Hydrophobic Polymer Blocks

Ahlam Alalwiat,[a] Sarah E. Grieshaber,[b,‡] Bradford A. Paik,[b] Kristi L. Kiick,[b] Xinqiao Jia[b] and Chrys Wesdemiotis*[,a]

[a] Department of Chemistry, The University of Akron, Akron, OH 44325-3601, USA. E-mail: wesdemiotis@uakron.edu; Fax: +1-330-972-6085; Tel.: +1-330-972-7699.

[b] Department of Materials Science and Engineering, University of Delaware, Newark, DE 19716.

† Electronic supplementary information (ESI) available.

‡ Current affiliation: SABIC Innovation Plastics, 1 Lexan Lane, Mount Vernon, IN 47620.

Abstract: A multidimensional mass spectrometry (MS) methodology is introduced for the molecular level characterization of polymer-peptide (or polymer-protein) copolymers that cannot be crystallized or chromatographically purified. It encompasses electrospray ionization (ESI) or matrix-assisted laser desorption ionization (MALDI) coupled with mass analysis, tandem mass spectrometry (MS^2) and gas-phase separation by ion mobility mass spectrometry (IM-MS). The entire analysis is performed in the mass spectrometer ("top-down" approach) within milliseconds and with high sensitivity, as demonstrated for hybrid materials composed of hydrophobic poly(*tert*-butyl acrylate) (P*t*BA) or hydrophilic poly(acrylic acid) (PAA) blocks tethered to the hydrophobic decapeptide VPGVGVPVGVG (VG2) via triazole linkages. The composition of the major products can be rapidly surveyed by MALDI-MS and MS^2. For a more comprehensive characterization, the ESI-IM-MS (and MS^2) combination is more suitable, as it separates the hybrid materials based on their unique charges and shapes from unconjugated polymer and partially hydrolyzed products. Such separation is essential for reducing spectral congestion, deconvoluting overlapping compositions and enabling straightforward structural assignments, both for the hybrid copolymers as well as the polymer and peptide reactants. The IM dimension also permits the measurement of collision cross-sections (CCSs), which reveal molecular architecture. The MS and MS^2 spectra of the mobility separated ions conclusively showed that $[PtBA–VG2]_m$ and $[PAA–VG2]_m$ chains with the expected compositions and sequences were formed. Single and double copolymer blocks (m = 1-2) could be detected. Further, the CCSs of the hybrids, which were prepared via azide/alkyne cycloadditions, confirmed the formation of macrocyclic structures. The top-down methodology described would be particularly useful for the detection and identification or peptide/protein-polymer conjugates which are increasingly used in biomedical and pharmaceutical applications.

Introduction

A new research area that has been developed in the last few years involves coupling poly(amino acid)s or peptides with designed sequences with synthetic polymers to create new materials known as polymer-peptide conjugates, hybrid materials or bioactive materials.[1,2] Many peptides have been approved as drugs because of several useful properties, including their ability to self-assemble into precisely defined structures and respond to external stimuli.[3] Peptide drugs with diverse conformations and functionalities can be prepared that show remarkable selectivity and specificity in their interactions with their targets.[3] Despite such advantages, the use of peptides in biomedical research is still limited because of certain adverse physical properties, including susceptibility to degradation and sensitivity to temperature, pH and organic solvents. These problems can be overcome by attaching a synthetic polymer to peptides, which helps to control their physical and chemical properties, such as viscosity and responsiveness to external stimuli (smart behavior).[3]

Peptides have been covalently attached to polymers using the succinimide, Schiff base, thiol-maleimide and click chemistry coupling methods.[4-6] A widely used click chemistry reaction is the azide-alkyne Huisgen cycloaddition, in which terminal azide groups react with terminal alkyne groups in the presence of a copper catalyst to produce triazole rings via 1,3-dipolar cycloaddition.[6-11] The advantages of this reaction are high efficiency, high selectivity, ease of product purification and compatibility with a wide diversity of functional groups.[4,12]

Many synthetic polymers have been successfully joined to peptides, including poly(ethylene glycol),[13-21] polystyrene[11,22-24] and poly(butyl acrylate).[25-28] Meanwhile, synthetic polypeptides derived from elastin have been used widely in drug delivery and tissue engineering, either by themselves or conjugated with a polymer.[29-31]

Elastin is a protein that affords flexibility to connective tissues, blood vessels, lungs and the skin of vertebrates.[32-35] This protein has two alternating domains. The first domain is rich in hydrophobic amino acids (Gly, Ala, Val and Pro) and it is the peptide sequence that endows flexibility to the tissues. The second domain is hydrophilic, enriched with Ala and Lys, and makes cross-links to other polypeptide chains with its Lys residues.[34,36] The structure of genetically engineered elastin-like polypeptides with the sequence $(VPGVG)_n$ changes from hydrophilic random coil to hydrophobic β-spiral when the temperature is increased because of inter- and intramolecular hydrogen bonding interactions. Changes in $(VPGVG)_n$ also affect any polymer coupled with it, even with only one repeat unit of the polypeptide.[37-39]

Although peptide-polymer conjugates are a fast growing field, their characterization is difficult because their solubility and polydispersity limit the analytical techniques suitable for the examination of their structures.[6] Literature about the molecular structure characterization of hybrid materials is limited. Peptide-polystyrene conjugates have been analyzed by UV spectroscopy, gel permeation chromatography (GPC), proton NMR and matrix-assisted laser desorption/ionization time-of-flight mass spectrometry (MALDI-ToF-MS).[24] Peptide-poly(ethylene glycol) (PEG) conjugates have been analyzed more widely by a variety of methods, including proton NMR,[1,40,41] GPC,[41] FTIR,[41] MALDI-ToF-MS,[1,40] Fourier transform ion cyclotron resonance mass spectrometry (FTICR-MS)[42,43] and electrospray ionization coupled with quadrupole/time-of-flight (Q/ToF) ion mobility mass spectrometry (IM-MS).[42] Finally the self-assembly of peptides conjugated to polyacrylates and polyacrylamides has been investigated by NMR,[44] GPC,[44,45] FTIR,[45-48] transmission electron microscopy[47,48] as well as electron[46] and x-ray[48] diffraction measurements.

In this study, top-down mass spectrometry methods[49-57] are introduced as a tool for the comprehensive characterization of hybrid materials that are difficult to solubilize, crystallize and/or purify, a prerequisite for most spectroscopic methods of analysis. The experimental approach is illustrated for an elastin mimicking hybrid copolymer composed of hydrophilic poly(acrylic acid) (PAA) blocks attached to blocks of the hydrophobic peptide VPGVGVPGVG (VG2), viz. $[PAA–VG2]_m$, and its synthetic precursor which contained hydrophobic poly(*tert*-butyl acrylate) (P*t*BA) instead of PAA.[58] The VG2 peptide and poly(acrylic acid) are also characterized individually. The methods used include MALDI-ToF-MS and MS^2 and ESI-Q/ToF-MS and MS^2 coupled with ion mobility separation (IM-MS).[59-62] All experiments are performed in the mass spectrometer without prior derivatization, digestion or chromatographic fractionation, qualifying this approach as a top-down MS methodology.[49-57] In addition, molecular modeling is employed to simulate the structures and collision cross-sections of the peptide-polymer conjugates for comparison with experimental results obtained by IM-MS in order to ascertain the architecture (linear vs. cyclic) of the synthesized hybrid materials. As will be documented here, the ion mobility dimension is essential for the structural identification of compounds which may exist in isomeric forms that cannot be effectively separated from each other or from the corresponding starting materials and/or byproducts.

Experimental

Materials

The synthetic pathways to the peptide, polymer and hybrid copolymers examined have been reported in detail elsewhere.[17,41,58] The alkyne functionalized peptide X(VG2)X, where X =

propargyl glycine, was prepared following standard solid phase peptide synthesis protocols, yielding a peptide that was acetylated at the N-terminus and amidated at the C-terminus.

The PAA sample analyzed was prepared as outlined in Scheme S1. Briefly, *tert*-butyl acrylate was polymerized by atom transfer radical polymerization (ATRP), using dimethyl 2,6-dibromoheptanedioate as telechelic initiator, to form poly(*tert*-butyl acrylate) dibromide. Subsequent reaction with sodium azide led to poly(*tert*-butyl acrylate) diazide (P*t*BA) which was hydrolyzed with trifluoroacetic acid to yield poly(acrylic acid) diazide (PAA).

The synthetic route to the hybrid materials examined is shown in Scheme 1. The synthesis of $[P\textit{t}BA–VG2]_m$ and $[PAA–VG2]_m$ started with a click chemistry reaction involving azide-alkyne Huisgen cycloaddition between the azide groups of P*t*BA and alkyne groups of VG2. In the presence of copper (I) acetate catalyst, 1,3-dipolar cycloaddition takes place between the terminal alkynes and azides to form the hybrid multiblock copolymer $[P\textit{t}BA–VG2]_m$ whose *tert*-butyl esters were subsequently hydrolyzed with trifluoroacetic acid (TFA) to form the hybrid material $[PAA–VG2]_m$ (Scheme 1). Step growth polymerization inevitably gives rise to cyclic oligomers, along with the linear counterparts of different molecular mass; the linear and cyclic structures of $[PAA–VG2]_m$ have the same molecular mass and both could contain one or more constituent blocks. For simplicity, only the linear structures of the hybrid materials were drawn in Scheme 1.

The reagents and solvents needed for the syntheses and mass spectrometry characterizations were purchased from Sigma-Aldrich (St. Louis, MO), VWR (Radnor, PA) or Fisher Scientific (Pittsburgh, PA), unless noted otherwise; all were used in the condition received.

MALDI-MS and MS^2 experiments

MS and MS^2 experiments were performed on a Bruker UltraFlex III MALDI-ToF/ToF mass spectrometer (Bruker Daltonics, Billerica, MA) equipped with a Nd:YAG laser emitting at 355 nm. The instrument was operated in positive or negative ion mode. With each sample, several matrices and cationizing salts were examined and those maximizing the signal-to-noise ratio and minimizing fragmentation were selected for the experiments described below.

The VG2 peptide was analyzed using the sandwich method and α-cyano-4-hydroxycinnamic acid (CHCA) as matrix. The CHCA matrix and sodium trifluoroacetate (NaTFA) salt were dissolved in THF at 20 mg/mL and 10 mg/mL, respectively, and the peptide was dissolved in DMSO at 10 mg/mL. Matrix and salt solutions were mixed at a volume ratio of 100:10 and this mixture was used to deposit the bottom and top layers of the sandwich-shaped sample analyzed, whereas the peptide solution was deposited as the middle layer. This sample preparation procedure led to the formation of $[VG2 + Na]^+$ ions.

For poly(acrylic acid) (PAA), CHCA and sinapinic acid (SA) served as matrices in positive and negative ion mode, respectively. Solutions of CHCA in THF and of SA in ACN:H_2O (70:30, vol%) were prepared at 20 mg/mL. A solution of NaTFA salt was prepared in THF at 10 mg/mL and mixed with the CHCA matrix solution at a volume ratio of 10:1. The polymer (PAA) was dissolved in THF or THF:MeOH (50:50, vol%) at 10 mg/mL. Matrix/salt and sample solutions were applied onto the MALDI target plate by the sandwich method. This sample preparation protocol led to mainly $[M + Na]^+$ ions in positive mode and mainly $[M - H]^-$ ions in negative mode.

DCTB, viz. {trans-2-[3-(4-*tert*-butylphenyl)-2-methyl-2-propenyldene] malononitrile, was the matrix used for the $[P\textit{t}BA–VG2]_m$ hybrid material in positive ion mode. THF solutions

of the matrix (20 mg/mL) and potassium trifluoroacetate (KTFA) salt (10 mg/mL) were mixed at a volume ratio of 10:1 and the resulting mixture was used for the top and bottom layers of the sandwich deposition method. A solution of $[P\textit{t}BA\text{-}VG2]_m$ (10 mg/mL) in a 25:75 (vol%) mixture of ammonium acetate buffer (pH = 6.64) and MeOH was used for deposition of the middle layer. This sample preparation protocol produced predominantly $[M + K]^+$ ions.

The $[PAA–VG2]_m$ hybrid material was analyzed in positive and negative ion modes with the CHCA matrix. Solutions of the matrix in THF (20 mg/mL) and $[PAA–VG2]_m$ in DMSO (20 mg/mL) were applied to the MALDI target via the sandwich method, which gave rise mainly to $[M + Na]^+$ ions in positive mode and $[M - H]^-$ ions in negative mode.

MALDI-MS^2 experiments were performed using Bruker's LIFT (laser-induced fragmentation) mode with no additional gas.[63] Data analysis was conducted with the flexAnalysis software.

ESI-IM-MS and MS^2 experiments

MS and MS^2 experiments were performed on a Waters Synapt HDMS quadrupole/time-of-flight (Q/ToF) mass spectrometer (Waters, Beverly, MA), equipped with an ESI source, operable in positive or negative ion modes, and with the traveling-wave variant of ion mobility mass spectrometry (IM-MS).[64,65] The sample solution was introduced to the ESI source by direct infusion at a flow rate of 3 μL/min. The instrument was operated in positive ion mode with a capillary voltage of 3.15 kV, cone voltage of 35 V, sampling cone voltage of 3.2 V, source temperature of 80 °C and desolvation temperature of 150º C. The instrument was operated in

negative ion mode with a capillary voltage of 1.66 kV, cone voltage of 51 V, sampling cone voltage of 1.1 V, source temperature of 80 °C and desolvation temperature of 150º C.

The infused solutions were prepared as follows: VG2 was dissolved in 0.056 M aqueous ammonium acetate buffer or in an aqueous 0.01-mg/mL solution of n-dodecyl-α-D-maltoside (Affymetrix, Santa Clara, CA) at 0.05 mg/mL and 10 vol% of MeOH was added to this solution to help buffer evaporation. PAA was dissolved in THF:MeOH (50:50, vol%) at 0.1 mg/mL, with 1 vol% formic acid added to aid ionization. The $[P\textit{t}BA–VG2]_m$ hybrid was dissolved in a 50:50 (vol %) mixture of ammonium acetate buffer and MeOH at the concentration of 0.1 mg/mL and 1 vol% formic acid was added to this solution to facilitate protonation. The $[PAA–VG2]_m$ hybrid was dissolved in ammonium acetate buffer at 0.01 mg/mL and 10 vol% MeOH was added to help the buffer evaporate. The instrument was operated in positive ion mode for the peptide and $[P\textit{t}BA–VG2]_m$ and in either positive or negative ion mode for PAA and $[PAA–VG2]_m$.

IM-MS measurements were conducted in the tri-wave region of the instrument, located between the Q and ToF mass analyzers and consisting of three confined chambers in the order trap cell (closest to Q), IM cell and transfer cell (closest to ToF). Nitrogen flows through the IM cell and argon through the trap and transfer cells. The nitrogen (drift gas) and argon (collision gas) flow rates were 22.7 mL/min and 1.5 mL/min, respectively. The traveling wave velocity in the IM cell was set at 350 m/s, and the corresponding traveling wave height was tuned to 12 V for VG2 and 8 V for PAA and the hybrid materials. Traveling wave height and traveling wave velocity were set at 0.5 V and 300 m/s, respectively, in the trap cell and at 0.2 V and 248 m/s, respectively, in the transfer cell. MS^2 experiments via collisionally activated dissociation (CAD) were performed in the transfer cell by raising the potential of this cell (bias) to 60 V.

Molecular modeling

Molecular mechanics/dynamics calculations were performed using the Materials Studio (version 7.0) program (Accelrys Software, Inc.). For each composition and architecture, 50 candidate structures were considered. Each initially energy-minimized structure was subjected to 50 annealing cycles with starting and midcycle temperatures of 50 and 1400 K, respectively, 20 heating ramps per cycle, 1000 dynamics steps per ramp and one dynamics step per femtosecond. The collision cross-sections of the resulting optimized structures were calculated by the projection approximation method available in the MOBCAL suite of programs.[66]

Results and discussion

Characterization of VG2 peptide

VG2 is a hydrophobic peptide with ten amino acid residues. These include four glycine units (G = $C_2H_3O_1N_1$ = 57.0214 Da), four valine units (V = $C_6H_9O_1N_1$ = 99.0684 Da) and two proline units (P = $C_6H_7O_1N_1$ = 97.0527 Da). Based on the synthetic route used to prepare VG2, its sequence should be XVPGVGVPGVGX where X is acetylated propargyl glycine ($C_7H_8O_2N_1$ = 138.0555 Da) at the N-terminus and amidated propargyl glycine ($C_5H_7O_1N_2$ = 111.0558 Da) at the C-terminus. The calculated mass of the combined end groups and the entire peptide are 249.11 and 1067.58 Da, respectively, using the monoisotopic masses of the elements in the peptide. The peptide is hydrophobic and could only be dissolved in DMSO and in aqueous ammonium acetate buffer or aqueous alkyl glycoside surfactant with a pH > 5.

MALDI-ToF/ToF-MS and MS^2 analysis. Fig. 1a shows the MALDI mass spectrum of VG2 acquired using a DMSO solution. The most abundant peak arises from the sodiated

peptide, $[VG2 + Na]^+$, at *m/z* 1090; the other ions originate from incomplete sequences. The desired sequence, $X(VPGVG)_2X$, and the reverse sequence, $X(GVGPV)_2X$, are isomers with equal molecular weights. Since both sequences have been investigated as elastin mimics,[37-39] tandem mass spectrometry was utilized to confirm the VG2 structure prepared in this study.

The MALDI-MS^2 spectrum of $[VG2 + Na]^+$ (*m/z* 1090), shown in Fig. 1b, agrees well with the sequence XVPGVGVPGVGX, comprising an acetylated propargyl glycine at the N-terminus and an amidated propargyl glycine at the C-terminus. The most abundant fragments belong to series a_n and y_n. According to established peptide ion fragmentation mechanisms,[67-69] these fragments are generated by rearrangement fragmentations at the C(=O)–NH bonds which break the peptide into two segments, one containing the N-terminus and the other the C-terminus. Retention of the Na^+ charge by the C-terminal segment gives rise to the y_n series, whereas charge retention by the N-terminal segment and concomitant CO loss gives rise to the a_n series. The intensity of fragments y_9 and a_6 is particularly high, indicating enhanced cleavage of the C(C=O)–NH bonds N-terminal to proline, as also found for protonated peptides.[70] The sodium ion affinities of proline (196 kJ/mol),[68] valine (173 kJ/mol)[68] and glycine (161 kJ/mol)[68] follow the same order as the corresponding proton affinities (921, 911 and 887 kJ/mol, respectively[71]). The enhanced peptide bond cleavage N-terminal to proline could thus result from high stabilization of the charge by the N-terminal proline unit created during such dissociation. The spectral features of the MALDI-MS^2 spectrum, viz. a complete y_n series from y_{10} to y_1, and intense a_n ions with longer chains (a_6, a_9), further suggest a preference for sodium ion coordination near the C-terminal residues.[72,73]

ESI-MS, ESI-IM-MS and MS^2 analysis. ESI of a VG2 solution in ammonium acetate buffer (pH = 6.64) produces mainly doubly charged ions, including $[VG2 + 2H]^{+2}$ (*m/z* 534.8),

$[VG2 + H + Na]^{+2}$ (545.8) and $[VG2 + 2Na]^{+2}$ (556.8), cf. Fig. S1. The intensities of the singly charged ions formed, which comprise $[M + H]^+$, $[M + NH_4]^+$ and $[M + Na]^+$ (*m/z* 1068.6, 1085.6 and 1090.6, respectively), are very low. The ESI mass spectrum also contains several singly protonated fragment ions, like y_1, y_4, a_5 and y_9, which are ascribed to collisionally activated dissociation (CAD) of $[M + 2H]^{+2}$ in the interface region between the ion source and the vacuum system.

Fig. 2 shows that IM-MS removes chemical noise and separates the intact peptide with one and two charges from fragments. The drift time for the singly charged ions is about 4 ms, while that for the doubly charged ions is about 1 ms. In either charge state, each intact peptide ion shows a single drift time distribution (see drift time chromatogram for $[VG2 + Na]^+$ in Fig. 2d), consistent with only one sequence and one structure.

Lipophilic peptides and even lipid membranes are readily dissolved in aqueous solutions of surfactants, such as n-dodecyl-α-D-maltoside (α-$C_{12}G_2$).[74-76] The latter surfactant was also used in this study to dissolve the hydrophobic VG2 peptide in H_2O/MeOH. The surfactant solution (0.01 mg/mL or 0.020 mM) was first analyzed separately to determine the background ions formed without the peptide. The major ions formed from pure surfactant are $[\alpha\text{-}C_{12}G_2 + Na]^+$ at *m/z* 533.4 and $[(\alpha\text{-}C_{12}G_2)_2 + Na]^+$ at *m/z* 1043.8. When the surfactant concentration in the sprayed solution was equal or higher than the concentration of the VG2 peptide, both VG2 and the surfactant components were detected. Conversely, when the concentration of VG2 was higher than that of the surfactant, only peptide ions were detected in the ESI mass spectrum, as attested in Fig. S2 for a 0.047-mM solution of VG2 in 0.020-mM aqueous α-$C_{12}G_2$ (+10% MeOH). This spectrum contains dominant singly charged ions with the compositions $[VG2 + H]^+$, $[VG2 + NH_4]^+$, $[VG2 + Na]^+$ and $[VG2 + K]^+$, as well as less abundant doubly charged

ions with the compositions $[VG2 + H + K]^{+2}$, $[VG2 + 2Na]^{+2}$, $[VG2 + 2Na]^{+2}$ and $[VG2 + Na + K]^{+2}$.

Comparison of the ESI-MS and IM-MS data for VG2 obtained using ammonium acetate buffer (Figs. S1 and 2a, respectively) and surfactant solution (Figs. S2 and 3a, respectively) reveals that the intensity of singly charged ions is higher with the surfactant solution, as is the corresponding drift time (4.60 ms vs. 4.15 ms with the buffer solution). Hence, using the surfactant solution reduces the degree of multiple charging and the compactness (folding) of VG2, presumably because the surfactant attracts ions attached to folded VG2 (preferentially Na^+), thereby lowering the charge state and weakening intramolecular hydrogen bonds in the peptide relative to ammonium acetate.[77] Fig. 3a shows the 2-D IM-MS^2 plot of $[VG2 + Na]^+$ (*m/z* 1090) and Fig. 3b the MS^2 spectrum extracted from this plot. The same y_n and a_n fragment ions are detected if the buffer is used to dissolve the VG2 peptide. Using the surfactant solution of the hydrophobic peptide affected the charge distribution and drift time but did not change the fragmentation pathways. All MS^2 spectra of VG2 (MALDI-MS^2 and ESI-IM-MS^2 using different solutions) confirm the VG2 peptide sequence and end groups.

Characterization of PAA homopolymer

The poly(acrylic acid) sample investigated (Scheme S1) has diazide end groups ($2xN_3$ = 84.0184 Da) and a central group composed of one methylene plus two methyl acrylate moieties ($C_9H_{14}O_4$ = 186.0892 Da). The total mass contributed by the central and chain end substituents is 270.11 Da.

MALDI-ToF-MS analysis. A major series with the PAA repeat unit ($C_3H_4O_2$, 72 Da) is clearly visible in the MALDI mass spectra obtained in positive (Fig. 4a) or negative (Fig. 4b) ion mode. These series arise from sodiated or deprotonated oligomers of PAA, respectively. Their *m/z* values agree well with the composition $(C_3H_4O_2)_n + C_9H_{14}O_4N_6$ (270 Da), confirming that complete hydrolysis of poly(*tert*-butyl acrylate) (P*t*BA) to PAA took place and that the resulting PAA contained the desired central substituent and diazide end groups. In positive mode, several minor distributions are observed due to exchange of the COOH proton with Na^+ or K^+. Ion intensities are much higher in negative ion mode than in positive ion mode pointing out that proton loss from PAA during MALDI is more efficient than the gain of a sodium ion.

ESI-MS and ESI-IM-MS analysis. ESI-MS of PAA leads to complex spectra showing ions in multiple charge states both in positive and negative modes. Mainly doubly charged ions are observed in positive and doubly or triply charged ions in negative ion mode. Spectral complexity is reduced by IM-MS, with which the PAA ions can be separated according to their charge as well as from chemical and contamination noise with repeat units of 28 and 44 Da (cf. Figs. 5 and S3).

The dominant ion series in the mass spectrum extracted from the mobility region of +2 ions (Fig. 5) corresponds to doubly potassiated oligomers, $[M + 2K]^{+2}$, which appear with a distance of 36 *m/z* units between successive n-mers, in keeping with the doubly charged PAA repeat unit ($C_3H_4O_2$, 72 Da). In negative ion mode (Fig. S3), the major series in the mass spectra extracted from the mobility regions of -2 and -3 ions arise from doubly deprotonated PAA oligomers and PAA oligomers that lost three protons and exchanged one additional proton with a K ion, respectively. Expectedly, triply charged ions have lower drift times than the doubly charged ions (Fig. S3). With either polarity, additional but relatively minor distributions are also

observed due to exchange of one or more COOH protons with Na and/or K. The *m/z* values of all positive and negative PAA ion series agree well with the composition $(C_3H_4O_2)_n$ + $C_9H_{14}O_4N_6$ (270 Da).

Characterization of [P*t*BA–VG2]$_m$ hybrid

The [P*t*BA–VG2]$_m$ hybrid polymer (Scheme 1) possesses a triazole-containing linking group at the N-terminal side of VG2 peptide (the molecular mass of this linking substituent, $C_7H_8O_2N_4$, is 180.0647 Da), a VG2 peptide segment with 10 amino acid residues (the molecular mass of VG2 peptide, $C_{38}H_{62}O_{10}N_{10}$, is 818.4649 Da), another triazole-containing linker as the C-terminal side of VG2 (the molecular mass of this linking group, $C_5H_7O_1N_5$, is 153.0651 Da) and a substituent in the center of the PAA segments containing the telechelic initiator used in the acrylate polymerization (the molecular mass of the center group, $C_9H_{14}O_4$, is 186.0892 Da). The mass of all substituents in the polyacrylate chain of one P*t*BA–VG2 block is equal to 1337.68 Da, resulting in a molecular weight distribution of 128n + 1338 Da per P*t*BA–VG2 constituent block (n = number of P*t*BA repeat units).

MALDI-MS data. The MALDI mass spectrum of [P*t*BA–VG2]$_m$ in positive ion mode (Fig. 6) includes a major series with the P*t*BA repeat unit ($C_7H_{12}O_2$, 128.0777 Da), arising from potassiated ions of [P*t*BA–VG2]$_1$ oligomers; the *m/z* values of all these ions, which are labeled by A_n in Fig. 6, agree well with the composition $(C_7H_{12}O_2)_n$ + $C_{59}H_{91}O_{17}N_{19}$ (1337.68 Da). A second series with the P*t*BA repeat unit is also clearly visible and this series arises from protonated ions of [P*t*BA–VG2]$_1$ oligomers that underwent exchange of the N_3 end group with a OCH_3 group. This exchange could occur during the synthesis or during the sample preparation process.[52]

GPC analysis indicated that $[PtBA–VG2]_m$ chains contain on average 3-6 copolymer blocks.[58] Multiple P*t*BA–VG2 blocks are, however, not detected upon MALDI, probably because of a significantly lower desorption and ionization efficiency as compared to $[PtBA–VG2]_1$. Nevertheless, the MALDI data unequivocally show that polymer-peptide conjugation took place to form a copolymer with the expected linking and end group substituents.

ESI-IM-MS analysis of P*t*BA–VG2. The ESI mass spectrum of $[PtBA–VG2]_m$ (positive ion mode) is complex, containing ions in multiple charge states from the desired product and unconsumed reactants. The $[PtBA–VG2]_m$ hybrid is observed doubly and triply charged. With IM-MS, these charge states are easily separated, as documented in Fig. 7. The mass spectrum extracted from the mobility separated doubly charged ions shows a dominant series with the P*t*BA repeat unit ($C_7H_{12}O_2$, 128 Da), corresponding to doubly protonated $[PtBA–VG2]_1$ oligomers, which appear every 128/2 = 64 *m/z* units. The *m/z* values of all these ions agree well with the composition $(C_7H_{12}O_2)_n + C_{59}H_{91}O_{17}N_{19}$ (1337.68 Da). Ion series with the P*t*BA repeat unit are also present in the mass spectrum extracted from the mobility separated triply charged region; here, the charges are provided by 3 protons and successive oligomers differing by one P*t*BA monomer are 128/3 = 42.67 *m/z* units apart from each other. The +3 region includes oligomers with the poly(acrylic acid) repeat unit ($C_3H_4O_2$, 72 Da), which appear every 72/3 = 24 *m/z* units. These are attributed to partial COO-*t*-C_4H_9 → COOH hydrolysis in the ammonium acetate buffer used to dissolve the P*t*BA–VG2 sample. Essentially all P*t*BA–VG2 oligomers observed in charge state +3 underwent partial *tert*-butyl ester hydrolysis. Oligomers with COOH pendants appear to protonate more easily than oligomers with completely esterified acrylate side chains, presumably because of more facile intramolecular H-bonding with the COOH as compared with the bulkier COO-*t*-C_4H_9 pendants. The architecture of P*t*BA–VG2

(linear vs. cyclic) and the presence and detection of multiple P*t*BA–VG2 blocks in the hybrid material (upon ESI) will be discussed later.

Characterization of $[PAA–VG2]_m$ hybrid

According to Scheme 1, the $[PAA–VG2]_m$ and $[P\textit{t}BA–VG2]_m$ hybrids have the same chain end, center and linking substituents. The total mass of these moieties is 1337.68 Da per polymer-peptide constituent block (vide supra). Further, the same moieties (and mass increment) would be present if the hybrid architecture is linear or macrocyclic (cf. Scheme 1).

MALDI-MS data. MALDI of $[PAA–VG2]_m$ gives rise to several ion series with the PAA repeat unit ($C_3H_4O_2$, 72 Da), both in negative (Fig. 8) as well as positive (Fig. S4) mode. The dominant distribution consists of deprotonated or sodiated oligomers of $[PAA–VG2]_1$, respectively, whose *m/z* values agree well with the composition $(C_3H_4O_2)_n + C_{59}H_{91}O_{17}N_{19}$ (1337.68 Da), indicating that a major fraction of P*t*BA underwent hydrolysis to PAA. In both modes, several minor distributions are observed due to remaining, un-hydrolyzed P*t*BA ester groups. It is noteworthy that complete hydrolysis was observed for the simple P*t*BA polymer with no peptide attachment (vide supra). Hydrogen bonding between the polymer and peptide blocks in $[P\textit{t}BA–VG2]_m$ and partially hydrolyzed $[PAA/P\textit{t}BA–VG2]_m$ most probably prevents the hydrolysis of all ester groups in the hybrid material.

ESI-IM-MS analysis of $[PAA–VG2]_m$. Under ESI conditions, $[PAA–VG2]_m$ forms doubly and triply charged cations (Fig. 9) or anions (Fig. S5). Using the ion mobility dimension, the hybrid material can be separated according to its charge as well as from unconjugated polymer (PAA and PAA/PtBA) and incompletely hydrolyzed hybrid (PAA/P*t*BA–VG2) in

various charge states. Such separation is imperative for reducing spectral congestion and enabling a straightforward spectral interpretation.

In positive ion mode (Fig. 9), the IM-MS spectrum extracted from the region of doubly charged PAA–VG2 shows just one series with the PAA repeat unit (72 Da), which arises from doubly protonated oligomers with one constituent block, viz. $[PAA–VG2]_1$. Oligomers differing by one repeat unit are separated by 72/2 = 36 *m/z* units, as expected for +2 ions; further, no P*t*BA content is detected beyond noise level. Very similar characteristics are present in the IM-MS spectrum extracted from the mobility region of triply charged PAA–VG2. Again, one series is observed, arising from triply protonated oligomers of PAA–VG2, which appear every 72/3 = 24 *m/z* units. Their *m/z* values correspond to hybrid material with one constituent block and no P*t*BA content. A third mobility area in the 2-D IM-MS plot (Fig. 9) contains PAA, PAA/P*t*BA and PAA/P*t*BA–VG2 in varying charges and looks particularly convoluted due to superimposed isobaric or nearly isobaric ions. A fourth mobility area, marked with an asterisk in Fig. 9a, contains +4 ions of $[PAA–VG2]_2$, which are more sensitively detected in IM-MS spectra acquired from individual, mass-selected oligomers (vide infra).

The measurements in negative ion mode give similar results. The major series in the IM-MS spectrum extracted from the region of doubly charged PAA–VG2 (Fig. S5), whose members appear at intervals of 72/2 = 36 *m/z* units, originates from doubly deprotonated oligomers with one constituent copolymer block. The same oligomers, triply deprotonated (every 72/3 = 24 *m/z* units), dominate in the spectrum extracted from the region of triply charged PAA–VG2. In both spectra, minor series due to one or more COOH → COOY (Y= K or Na) exchanges are also present. The *m/z* values of the major and minor ion series of doubly and triply deprotonated hybrid material corroborate the composition $(C_3H_4O_2)_n + C_{59}H_{91}O_{17}N_{19}$ (1337.68 Da). The two

other circled areas in the IM-MS plot in Fig. S5 include PAA, PAA/P*t*BA and PAA/P*t*BA–VG2 with different charges. In summary, both MALDI-MS and ESI-IM-MS confirm the expected of PAA–VG2 composition and the substituents incorporated in this material, with the most conclusive identification provided by the mobility separated species.

Insight on hybrid architecture from collision cross-sections

Derivation of collision cross-sections from traveling wave IM-MS experiments. From the drift time of an ion through the IM region, the corresponding collision cross-section (CCS or Ω) can be derived which is an important physical property, characteristic of the ion's size and conformation (shape). With traveling wave IM-MS, there is no direct relationship between the measured drift time (t_D) and Ω. Collision cross-sections are derived by calibrating the drift time scale with standards of known Ω, following a procedure that has been described in detail in the literature.[78-80] The calibration standards are ions with known Ω values, determined by the drift time ion mobility spectrometry (DTIMS) version of IM-MS,[59,61] in which a constant electric field is applied to an IM chamber filled with He. The buffer gas in traveling wave IM-MS experiments is usually N_2; it has been shown for ions of small and medium size ($\Omega < 600$ Å^2), however, that collision cross-sections deduced from such experiments by using calibrant Ω values obtained with He match within ±3% collision cross-sections measured directly with DTIMS.[78-80] Even for larger protein ions ($\Omega \approx 1200$-2600 Å^2), the collision cross-sections derived from the described calibration procedure and from DTIMS measurements agree reasonably well (within ca. ±10%).[81] The calibrants employed in this study were singly and doubly charged polyalanine oligomers[82] which, when analyzed under the same traveling wave velocity, traveling wave height and ion mobility drift gas (N_2) flow rate as the hybrid materials, lead to the calibration curve

depicted in Fig. S6; the data plotted to obtain this curve are listed in Table S1. The validity of the calibration curve in Fig. S6 was tested by using it to determine the CCSs of triply charged polyalanine oligomers and of several charge states of the proteins ubiquitin and cytochrome C, which were previously measured by DTIMS (Table S2).[82-85] Published CCS and experimental CCS obtained from the calibration plot differ on average by <3% for the polyalanine n-mers ($\Omega \approx 430\text{-}520$ Å^2) and by <9% for the ubiquitin and cytochrome C ions ($\Omega \approx 1500\text{-}2800$ Å^2). Given the relatively small size of the P*t*BA–VG2 and PAA–VG2 copolymers analyzed in this study, the error in their CCS values obtained from the calibration plot of Fig. S6 should by <4%.

Doubly and triply protonated P*t*BA–VG2 oligomers were isolated for IM-MS analysis. Fig. 10 shows the IM-MS drift time distribution ("IM-MS chromatogram") of mass-selected $[P\textit{t}BA_8\text{–}VG2]_1^{+2}$ at *m/z* 1182. It includes a single drift time distribution of +2 ions with one P*t*BA–VG2 block, consistent with one structure for such oligomers. There is a broad peak with low intensity at lower drift times, which is attributed to higher charge states containing more than one P*t*BA–VG2 constituent block. Similar results are obtained for other +2 or +3 ions of P*t*BA–VG2. Table 1 lists the drift times of nine doubly or triply protonated P*t*BA–VG2 oligomers together with their collision cross-sections, derived by using polyalanine as CCS calibrant (Fig. S6). Expectedly, the CCS increases with charge for the same oligomer due to stronger charge repulsion forces in the structure carrying more charges.

Several PAA–VG2 ions were also examined by IM-MS. Fig. 11a shows a representative IM-MS chromatogram, acquired from mass-selected *m/z* 1102 which corresponds nominally to doubly protonated $[PAA_{12}\text{–}VG2]_1$. Three peaks with three distinct drift times are observed, with the middle component having the highest intensity. The isotope patterns and *m/z* values in the mass spectra extracted from the mobility-separated peaks reveal that the center component

drifting at 5.96 ms arises from doubly protonated $[PAA_{12}–VG2]_1$. Its narrow peaks shape is consistent with one architecture which could be linear or cyclic (vide infra). Conversely, the component drifting at 4.06 ms is identified as the quadruply protonated copolymer with two constituent polymer-peptide blocks, viz. $[PAA_{12}–VG2]_2$. Finally, the most slowly drifting component, appearing at 7.13 ms, is assigned to mixtures of $[PAA_{11} + K]^+$ plus $[PAA_{26} + Na + K]^{+2}$ (unreacted polymer). IM-MS analysis of triply charged PAA–VG2 also indicates the presence of overlapping isobars, as exemplified in Fig. 11b for triply protonated $[PAA_{16}–VG2]_1$ (*m/z* 831). Here, the superimposed component is unreacted, longer chain PAA with overall +3 charges. The longer drift times of the unreacted PAA in Figs. 11a-b is attributed to its lower charge state (Fig. 11a) or to a longer polymer chain (compared to the PAA block in PAA–VG2) that lacks the peptide block which would have promoted folding and faster traveling motion in the IM cell.

Table 1 includes the drift times of twelve doubly and triply protonated PAA–VG2 oligomers with one constituent block and the collision cross-sections obtained from these data by using the calibration curve established with polyalanine (Fig. S6). In general, drift times and CCSs are lower for PAA–VG2 than for P*t*BA–VG2 oligomers with the same number of acrylate repeat units, because PAA lacks the bulky *tert*-butyl substituents and enables extensive hydrogen bonding interactions that generate more folded, compact structures (vide infra).

Theoretical collision cross-sections. The structure of the hybrid materials could be linear or cyclic depending on whether intramolecular cycloaddition between the chain ends occurs. To answer this question, computational modeling was used. Energy minimization of $[P*t*BA–VG2]_1$ and $[PAA–VG2]_1$ oligomers with different numbers of acrylate repeat units, 2-3 proton charges and linear or cyclic structures was performed by molecular mechanics/dynamics

simulations and the collision cross-sections of the resulting optimized structures were calculated by the projection approximation (PA) method. Fifty candidate structures per composition (n-mer) and architecture (linear or cyclic) were considered. The average Ω_{calcd} values obtained this way for each species are included in Table 1 and typical Ω_{calcd} vs. relative energy plots are shown in Fig. S7 for P*t*BA$_7$–VG2 and PAA$_{10}$–VG2**.**

Fig. 12 compares the calculated collision cross-sections of linear and cyclic P*t*BA–VG2 and PAA–VG2 oligomers in charge state +2 with the corresponding measured values. For P*t*BA–VG2 (Fig. 12a), the measured CCSs match within experimental error (~4%) the CCSs calculated for the cyclic structures indicating that all possible 1,3-cycloadditions have taken place and that the hybrid material contains solely triazole functionalities and no free azide and alkyne end groups. As with P*t*BA–VG2, the cyclic PAA–VG2 architectures are more compact and have smaller collision cross-sections than their linear analogs. In contrast to P*t*BA–VG2, however, the experimental CCSs do not match those of the macrocycles, but are even smaller. Very similar trends are observed for P*t*BA–VG2 vs. PAA–VG2 n-mers in charge state +3 (cf. Fig. S8). Since PAA–VG2 is formed from P*t*BA–VG2 (cf. Scheme 1) by *tert*-butyl ester hydrolysis, which does not affect triazole moieties, the final PAA–VG2 product must also be cyclic. The higher compactness (smaller CCS) of cyclic PAA–VG2, compared to the theoretical prediction, is attributed to the extensive hydrogen bond network formed with the COOH pendants of PAA chains and the VG2 amide groups. It is likely that the molecular mechanics/dynamics simulations miss some of the most compact PAA–VG2 conformations, leading to overestimated CCS values.

Conclusions

The results presented in this study showed how top-down MS, involving tandem MS and ion mobility mass spectrometry (IM-MS), can be used to characterize a derivatized synthetic peptide (complete end group and sequence analysis), a polymer and the corresponding polymer-peptide hybrid copolymer. Top-down MS is a new approach suitable for the analysis of complex materials that cannot be obtained in the high purity needed for structural characterization by other spectroscopic methods such as XRD and NMR. The top-down MS strategies discussed are fast, require very little material and can reveal information about both the compositional as well as the architectural microstructure of the material under study. Such methods should be particularly useful for the detection and identification of peptide-polymer and protein-polymer conjugates, which are increasingly used in biomedical and pharmaceutical research and applications.

Acknowledgements

We thank the National Science Foundation (CHE-1308307 to C.W.; DMR-0643226 to X.J.; CHE-1213728 to K.L.K. and X.J.) for generous financial support.

References

1. J. Y. Shu, C. Tan, W. F. DeGrado, T. Xu, *Biomacromolecules,* 2008, **9**, 2111-2117.
2. H. Robson Marsden and A. Kros, *Macromol. Biosci.*, 2009, **9**, 939-951.
3. I. R. Ruttekolk, A.Chakrabarti, M. Richter, F. Duchardt, H. Glauner, W. P. R. Verdurmen, J. Rademann and R. Brock, *Mol. Pharmacol.*, 2011, **79**, 692-700.

4. A. A. Sohdi, D. Campbell and P. D. Topham, *Chiang Mai J. Sci.*, 2012, **39**, 351-372.
5. J. Y. Shu, B. Panganiban and T. Xu, *Annu. Rev. Phys. Chem.*, 2013, **64**, 631-657.
6. S. Dehn, R. Chapman, K. A. Jolliffe and S. Perrier, *Polym. Rev.*, 2011, **51**, 214-234.
7. A. J. Dirks, S. S. van Berkel, N. S. Hatzakis, J. A. Opsteen, F. L. van Delft, J. J. L. M. Cornelissen, A. E. Rowan, J. C. M. van Hest, F. P. J. T. Rutjes and R. J. M. Nolte, *Chem. Commun.*, 2005, **33**, 4172-4174.
8. V. V. Rostovtsev, L. G. Green, V. V. Fokin and K. B. Sharpless, *Angew. Chem.*, 2002, **114**, 2708-2711.
9. S. Dedola, S. A. Nepogodiev and R. A. Field, *Org. Biomol. Chem.*, 2007, **5**, 1006-1017.
10. J.-F. Lutz, *Angew. Chem. Int. Ed.*, 2007, **46**, 1018-1025.
11. G. C Tron, T. Pirali, R. A Billington, P. L Canonico, G. Sorba and A. A Genazzani, *Med. Res. Rev.*, 2008, **28**, 278-308.
12. J.-F. Lutz, H. G. Börner and K. Weichenhan, *Austr. J. Chem.*, 2007, **60**, 410-413.
13. M. Pechar, P. Kopečková, L. Joss and J. Kopeček, *Macromol. Biosci.*, 2002, **2**, 199-206.
14. J. H. Collier and P. B. Messersmith, *Adv. Mater.*, 2004, **16**, 907-910.
15. J. Hentschel, E. Krause and H. G. Börner, *J. Am. Chem. Soc.*, 2006, **128**, 7722–7723.
16. I. W. Hamley, M. J. Krysmann, V. Castelletto and L. Noirez, *Adv. Mater.*, 2008, **20**, 4394-4397.
17. S. E. Grieshaber, A. J. Farran, S. Lin-Gibson, K. L. Kiick and X. Jia, *Macromolecules*, 2009, **42**, 2532-2541.
18. H. Kühnle and H. G. Börner, *Angew. Chem. Int. Ed.*, 2009, **48**, 6431-6434.
19. A. Verch, H. Hahn, E. Krause, H. Cölfen and H. G. Börner, *Chem. Commun.*, 2010, **46**, 8938-8940.

20. M. Chenal, C. Boursier, Y. Guillaneuf, M. Taverna, P. Couvreur and J. Nicolas, *Polym. Chem.*, 2011, **2**, 1523-1530.

21. W. Tang, Y. Ma, S. Xie, K. Guo, B. Katzenmeyer, C. Wesdemiotis and M. L. Becker, *Biomacromolecules*, 2013, **14**, 2204-3313.

22. B. Le Droumaguet and K. Velonia, *Angew. Chem.*, 2008, **120**, 6359-6362.

23. J. Y. Shu, Y.-J. Huang, C. Tan, A. D. Presley, J. Chang and T. Xu, *Biomacromolecules*, 2010, **11**, 1443-1452.

24. T. Trimaille, K. Mabrouk, V. Monnier, L. Charles, D. Bertin, D. Gigmes, *Macromolecules*, 2010, **43**, 4864-4870.

25. H. Rettig, E. Krause and H. G. Börner, *Macromol. Rapid Commun.*, 2004, **25**, 1251-1256.

26. M. G. J. ten Cate, N. Severin and H. G. Börner, *Macromolecules*, 2006, **39**, 7831-7838.

27. J. Hentschel, M. G. J. ten Cate and H. G. Börner, *Macromolecules*, 2007, **40**, 9224-9232.

28. S. Loschonsky, J. Couet and M. Biesalski, *Macromol. Rapid Commun.*, 2008, **29**, 309-315.

29. J. R. McDaniel, D. J. Callahan and A. Chilkoti, *Adv. Drug Delivery Rev.*, 2010, **62**, 1456-1467.

30. H. Arkin and M. Bilsel, *Eur. Phys. J. E.*, 2010, **31**, 327-332.

31. S. E. Grieshaber, T. Nie, C. Yan, S. Zhong, S. S. Teller, R. J. Clifton, D. J. Pochan, K. L. Kiick and X. Jia, *Macromol. Chem. Phys.*, 2011, **212**, 229-239.

32. L. Debelle and A. M. Tamburro, *Int. J. Biochem Cell B.*, 1999, **31**, 261-272.

33. B. Li, D. O. V. Alonso and V. Daggett, *J. Mol. Biol.*, 2001, **305**, 581-592.

34. X. L. Yao and M. Hong, *J. Am. Chem. Soc.*, 2004, **126**, 4199-4210.

35. C. Nicolini, R. Ravindra, B. Ludolph and R. Winter, *Biophys. J.*, 2004, **86**, 1385-1392.

36. R. Rousseau, E. Schreiner, A. Kohlmeyer and D. Marx, *Biophys. J.*, 2004, **86**, 1303-1407.

37. P. C. Gross, W. Possart and M. Zeppezauer, *Z. Naturforsch. C*, 2003, **58**, 873-878.

38. J. Reguera, M. Alonso, A. M. Testera, I. M. López, S. Martín, J. C. Rodríguez-Cabello, *Carbohyd. Polym.*, 2004, **57**, 293-297.

39. V. Lemieux, P. H. H. M. Adams and J. C. M. van Hest, *Method Mol. Biol.*, 2013, **991**, 353-362.

40. D. Elbert and J. Hubbell, *Biomacromolecules*, 2001, **2**, 430-441.

41. S. E. Grieshaber, A. J. E. Farran, S. Bai, K. L. Kiick and X. Jia, *Biomacromolecules*, 2012, **13**, 1774-1786.

42. D. Bagal, H. Zhang and P. D. Schnier, *Anal. Chem.*, 2008, **80**, 2408-2418.

43. R. R. Abzalimov, A. Frimpong and I. A. Kaltashov, *Int. J. Mass Spectrom.*, 2012, **312**, 135-143.

44. M. G. J. ten Cate, H. Rettig , K. Bernhardt and H. G. Börner, *Macromolecules*, 2005, **38**, 10643-10649.

45. M. L. Koh, K. A. Jolliffe and S. Perrier, *Biomacromolecules*, 2014, **15**, 2002-4011.

46. M. G. J. ten Cate, N. Severin and H. G. Börner, *Macromolecules*, 2006, **39**, 7831-7838.

47. J. Hentschel, M. G. J. ten Cate and H. G. Börner, *Macromolecules*, 2007, **40**, 9224-9232.

48. S. Dehn, V. Castelletto, I. W. Hamley and S. Perrier, *Biomacromolecules*, 2012, **13**, 2739-2747.

49. F. W. McLafferty, K. Breuker, M. Jin, X. Han, G. Infusini, H. Jiang, X. Kong and T. P. Begley, *FEBS J.*, 2007, **274**, 6256-6268.

50. N. Siuti, Nertila and N. L. Kelleher, *Nat. Methods*, 2007, **4**, 817-821.

51. G. Scherperel and G. E. Reid, *Analyst*, 2007, **132**, 500-506.

52. X. Li, G. Li, M. Casiano-Maldonado, D. Zhang and C. Wesdemiotis, *Macromolecules*, 2011, **44**, 4555-4564.

53. T. W. Mitchell, S. H. J. Brown and S. J. Blanksby, In *Lipidomics*, K. Ekroos (Ed.), Wiley-VCH: Weinheim, 2012, pp. 99-128.

54. F. Lanucara and C. E. Eyers, *Mass Spectrom. Rev.*, 2013, **32**, 27-42.

55. M. Helm and S. Kellner, *Nachr. Chem.*, 2013, **61**, 307-312.

56. E. B. Erba, *Proteomics*, 2014, **14**, 1259-1270.

57. K. Guo, Z. Guo, J. M. Ludlow III, T. Xie, S. Liao, G. R. Newkome and C. Wesdemiotis, *Macromol. Chem. Phys.*, 2015, **36**, 1539-1552.

58. S. E. Grieshaber, B. A. Paik, S. Bai, K. L. Kiick and X. Jia, *Soft Matter*, 2013, **9**, 1589-1599.

59. M. T. Bowers, P. R. Kemper, G. von Helden and P. A. M. van Koppen, *Science*, 1993, **260**, 1446-1451.

60. D. E. Clemmer and M. F. Jarrold, *J. Mass Spectrom.*, 1997, **32**, 577-592.

61. A. B. Kanu, P. Dwivedi, M. Tam, L. Matz and H. Hill Jr., *J. Mass Spectrom.*, 2008, **43**, 1-22.

62. C. L. Wilkins and S. Trimpin (Eds.), *Ion Mobility Spectrometry-Mass Spectrometry*, CRC Press: Boca Raton, 2011.

63. D. Suckau, A. Reseman, M. Schuerenberg, P. Hufnagel, J. Franzen and A. Holle, *Anal. Bioanal. Chem.*, 2003, **376**, 952-965.

64. K. Giles, S. D. Pringle, K. R. Worthington, D. Little, J. L. Wildgoose and R. H. Bateman, *Rapid Commun. Mass Spectrom.*, 2004, **18**, 2401-2414.

65. S. D. Pringle, K. Giles, J. L. Wildgoose, J. P. Williams, S. E. Slade, K. Thalassinos, R. H. Bateman, M. T. Bowers and J. H. Scrivens, *Int. J. Mass Spectrom.*, 2007, **261**, 1-12.

66. M. F. Mesleh, J. M. Hunter, A. A. Shvartsburg, G. C. Schatz and M. F. Jarrold, *J. Phys. Chem.*, 1996, **100**, 16082-16086.

67. K. B. Tomer, L. J. Deterding and C. Guenat, *Biol. Mass Spectrom.*, 1991, **20**, 121-129.

68. M. M. Kish, G. Ohanessian and C. Wesdemiotis, *Int. J. Mass Spectrom.*, 2003, **227**, 509-524.

69. B. Paizs and S. Suhai, *Mass Spectrom. Rev.*, 2005, **24**, 508-548.

70. M. D. M. Raulfs, L. Breci, M. Bernier, O. M. Hamdy, A. Janiga, V. H. Wysocki and J. C. Poutsma, *J. Am. Soc. Mass Spectrom.*, 2014, **25**, 1705-1715.

71. http://webbook.nist.gov/chemistry/ (accessed on 22 May2015).

72. B. A. Cerda, L. Cornett and C. Wesdemiotis, *Int. J. Mass Spectrom.*, 1999, **193**, 205-226.

73. M. Kohtani, M. F. Jarrold, S. Wee and R. A. J. O'Hair, *J. Phys. Chem. B*, 2004, **108**, 6093-6097.

74. H. Sjögren, C. A. Ericsson, J. Evenäs and S. Ulvenlund, *Biophys. J.*, 2005, **89**, 4219-4233.

75. N. P. Barrera, N. Di Bartolo, P. J. Booth and C. V. Robinson, *Science*, 2008, **321**, 243-246.

76. T. Ujihara, I. Sakurai, N. Mizusawa and H. Wada, *Anal. Biochem.*, 2008, **374**, 429-431.

77. M. G. Semenova, L. E. Belyakova, Y. N. Polikarpov, M. M. Il'in, T. A. Istarova, M. S. Anokhina and E. N. Tsapkina, *Biomacromolecules*, 2006, **7**, 101-113.

78. B. T. Ruotolo, J. Benesch, A. Sandercock, S.-J. Hyung and C.V. Robinson, *Nat. Protoc.*, 2008 **3**, 1139-1152.

79. K. Thalassinos, M. Grabenauer, S. E. Slade, G. R. Hilton, M. T. Bowers and J. H. Scrivens, *Anal. Chem.*, 2009, **81**, 248-254.

80. B. C. Katzenmeyer, L. R. Cool, J. P. Williams, K. Craven, J. M. Brown and C. Wesdemiotis, *Int. J. Mass Spectrom.*, 2015, **378**, 303-311.

81. D. P. Smith, T. W. Knapman, I. Campuzano, R. W. Malham, J. T. Berryman, S. E. Radford and A.E. Ashcroft, *Eur. J. Mass Spectrom.*, 2009, **15**, 113-130.

82. M. F. Bush, I. D. G. Campuzano and C. V. Robinson, *Anal. Chem.*, 2012, **84**, 7124-7130.

83. S. J. Valentine, A. E. Counterman and D. E. Clemmer, *J. Am. Soc. Mass Spectrom.*, 1997, **8**, 954-961.

84. K. B. Shelimov, D. E. Clemmer, R. R. Hudgins and M. F. Jarrold, *J. Am. Chem. Soc.*, 1997, **119**, 2240-2248.

85. http://www.indiana.edu/~clemmer/Research/Cross%20Section%20Database/Proteins/protein_cs.htm (accessed on 29 July 2015).

Table 1 Measured and calculated collision cross-sections (Ω) of doubly and triply protonated $[PtBA_n–VG2]_1$ and $[PAA_n–VG2]_1$ oligomers (n = number of P*t*BA or PAA repeat units)

z	n	*m/z*	t_D (ms)[a]	t_D' (ms)[b]	Ω' (Å^2)[c]	Ω (Å^2)[d]	Ω_{calcd} (Å^2)[e]	
							Cyclic	Linear
				$[PtBA_n–VG2]_1$				
2	4	926.05	5.50	5.529	957.35	365	367	388
2	6	1054.19	6.41	6.441	1041.32	396	396	428
2	7	1118.25	7.05	7.082	1097.17	417	411	444
2	8	1182.28	7.70	7.733	1152.07	438	430	458
2	10	1310.36	8.72	8.755	1233.00	468	464	499
3	5[f]	732.44	3.08	3.106	696.82	398	404	431
3	6[f]	775.17	3.33	3.356	727.27	415	416	449
3	7[f]	817.84	3.59	3.617	757.86	432	439	465
3	9[f]	903.23	4.00	4.029	804.18	458	469	501
				$[PAA_n–VG2]_1$				
2	7	921.97	4.75	4.779	838.49	336	352	376
2	8	957.39	4.89	4.920	897.71	342	366	395
2	10	1029.93	5.47	5.496	954.16	363	389	413
2	12	1101.95	5.96	5.992	1000.68	381	390	432
2	14	1174.07	6.28	6.313	1029.86	391	416	464
2	15	1209.98	6.39	6.418	1039.30	395	426	459
2	16	1246.45	6.93	6.964	1087.06	413	436	471
3	10	687.03	2.61	2.635	636.50	363	386	417
3	12	734.95	2.69	2.716	647.19	369	408	445
3	14	783.02	2.82	2.847	664.18	379	413	457
3	15	806.97	3.03	3.057	690.79	394	430	474
3	16	831.03	3.08	3.107	697.04	397	437	483

[a] Measured drift time. [b] Corrected drift time, $t_D' = t_D - [C(m/z)^{0.5}/1000]$ (C = 1.41 is a correction factor for instrument flight time effects). [c] Normalized CCS (Ω'), obtained from the calibration

equation shown in Fig. S6; $\Omega' = 373.33(t_D')^{0.5507}$. [d] Measured CCS ($\Omega$), $\Omega = \Omega'(z/\mu^{0.5})$ where z is the ion charge and μ is the reduced mass of the ion and drift gas (N_2). [e] Calculated by the projection approximation method from energy-minimized structures obtained by molecular mechanics/dynamics simulations (see text). [f] The triply protonated P*t*BA–VG2 oligomers also contain 3 hydrolyzed PAA repeat units in addition to the listed P*t*BA repeat units.

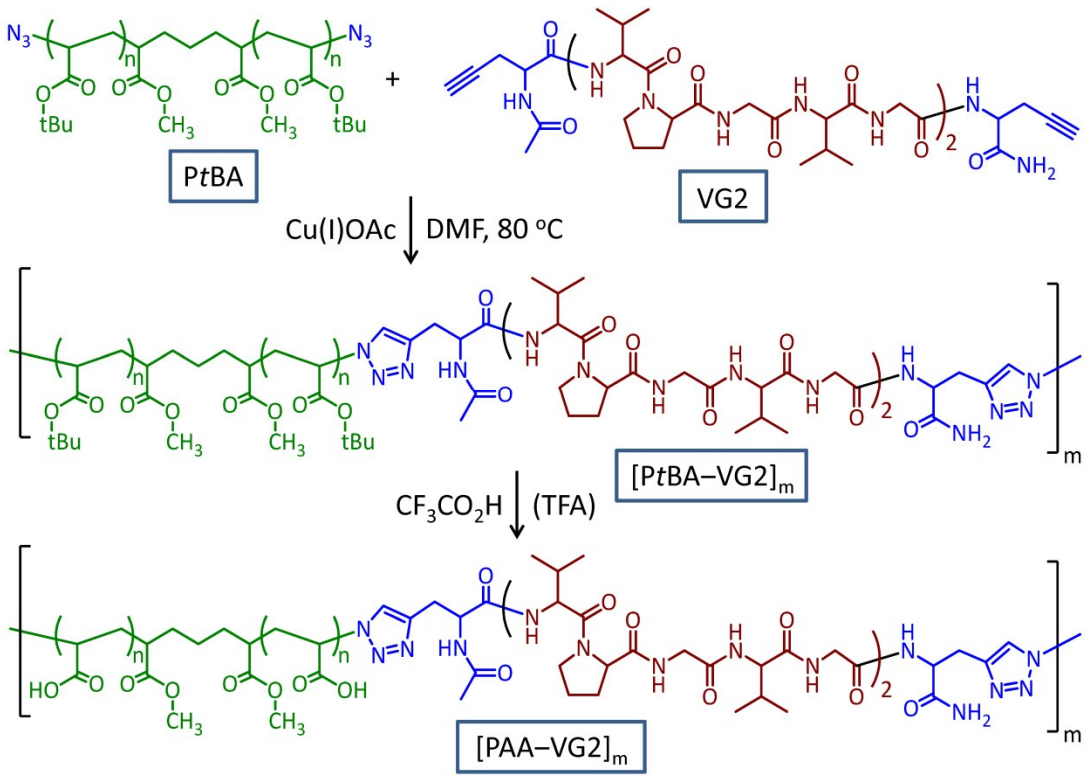

Scheme 1. Synthetic route to hybrid copolymers [P*t*BA–VG2]$_m$ and [PAA–VG2]$_m$, in which the polymer and peptide blocks are tethered through triazole linkages: $C_7H_8O_2N_4$, 180.0647 Da, at the N-terminal side of VG2; and $C_5H_7O_1N_5$, 153.0651 Da, at the C-terminal side of VG2. If the final structure is linear, the product carries either an amidated propargyl glycine ($C_5H_7O_1N_2$, 111.0558 Da) or an acetylated propargyl glycine ($C_7H_8O_2N_1$, 138.0555 Da) at the peptide chain end and an azide substituent (N_3, 42.0092 Da) at the polymer chain end. If the chain ends react to form a macrocycle, a new triazole functionality is generated that has the same composition and mass as one the two possible end group combinations in the linear architecture.

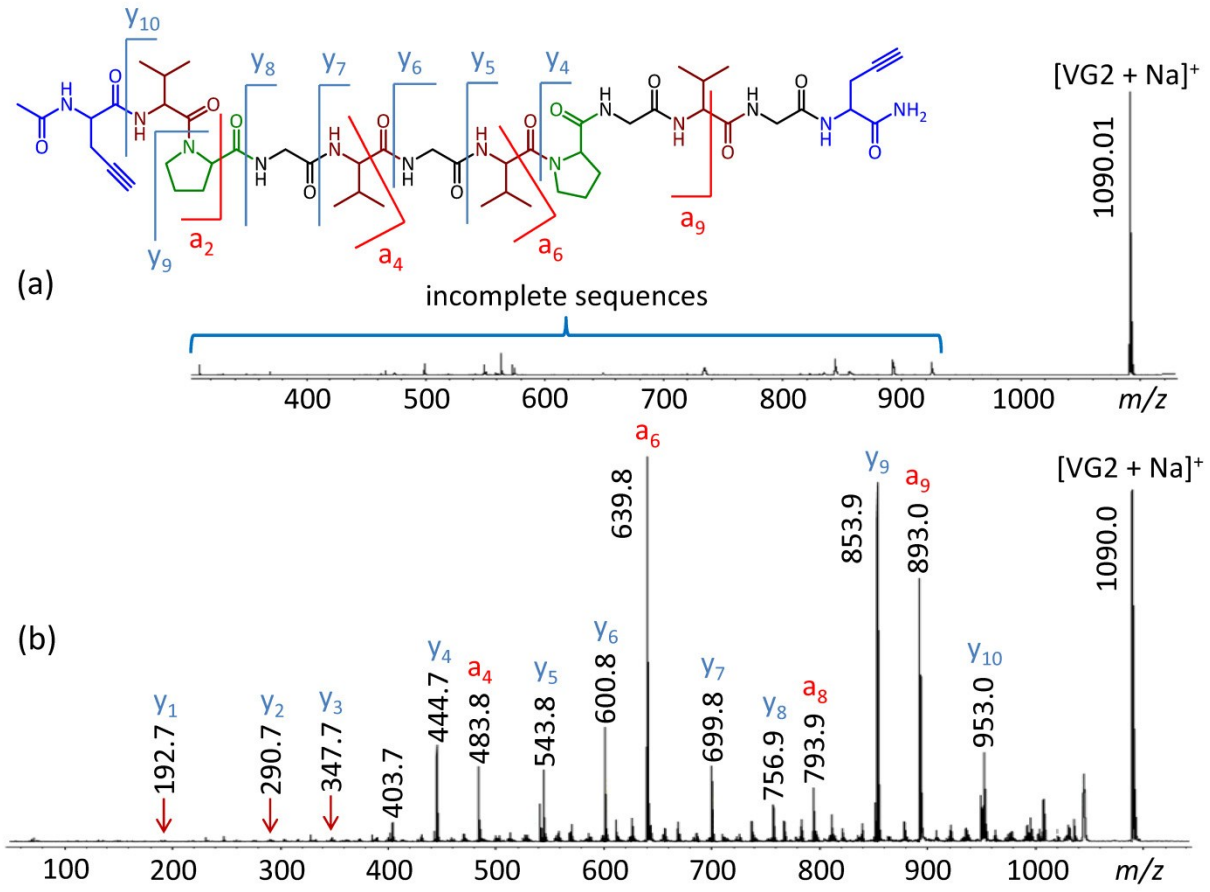

Fig. 1. (a) MALDI mass spectrum of VG2 peptide; (b) MALDI-MS^2 spectrum of sodiated VG2 (*m/z* 1090). The sequence of the peptide and the major N-terminal (a_n) and C-terminal (y_n) fragments are shown at the top.

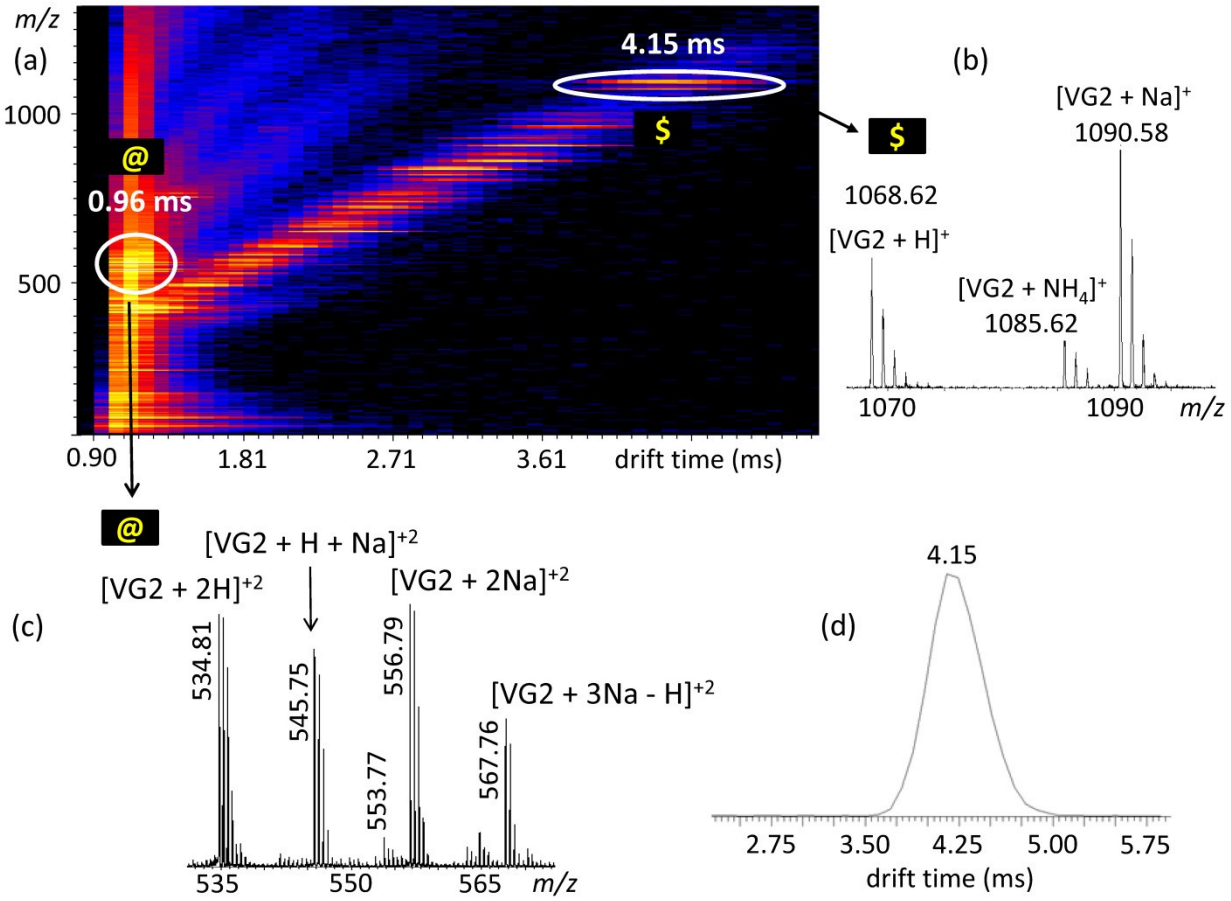

Fig. 2. (a) 2-D IM-MS plot (*m/z* vs. drift time) of VG2 dissolved in aqueous ammonium acetate; (b,c) mass spectra extracted from the IM regions of (a) singly and (b) doubly charged VG2 (labeled by $ and @, respectively); (d) drift time chromatogram (mobilogram) for $[VG2 + Na]^+$ (*m/z* 1090).

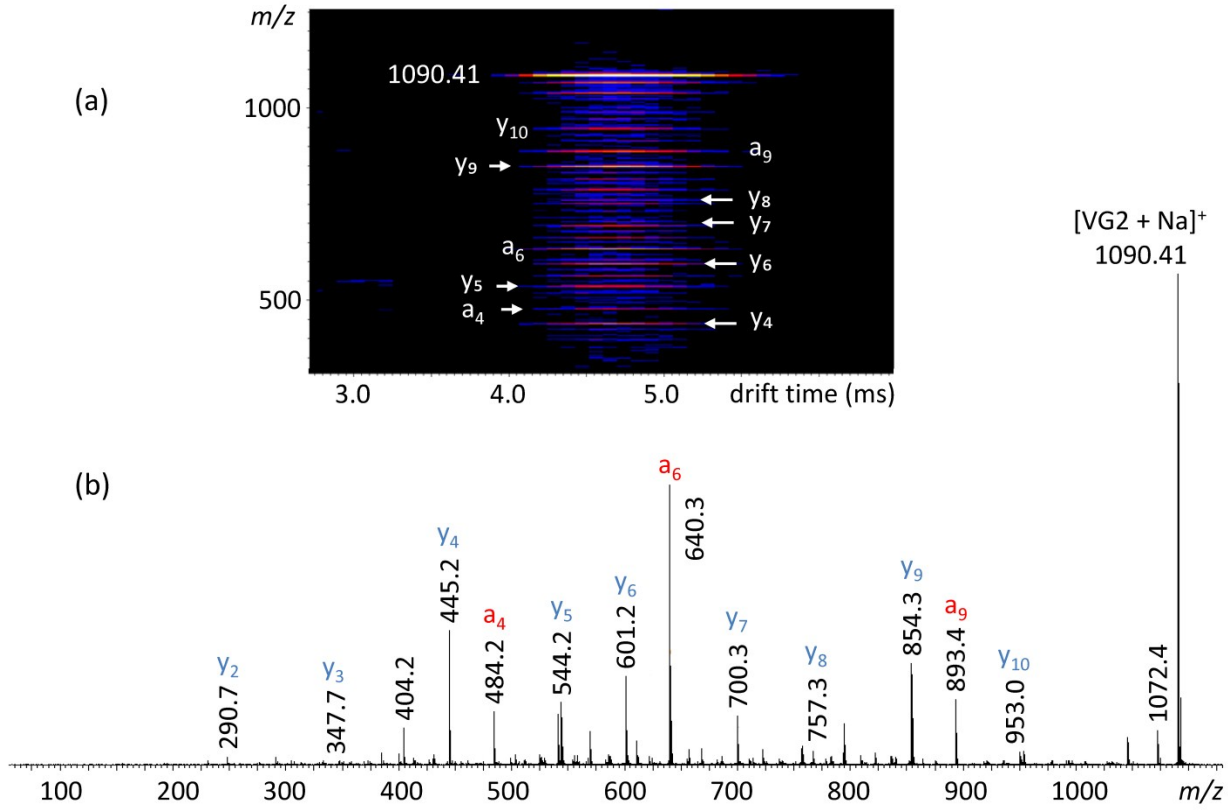

Fig. 3. (a) 2-D IM-MS^2 plot for [VG2 + Na]$^+$ (*m/z* 1090) and (b) extracted IM-MS^2 spectrum. VG2 was dissolved in aqueous n-dodecyl-α-D-maltoside.

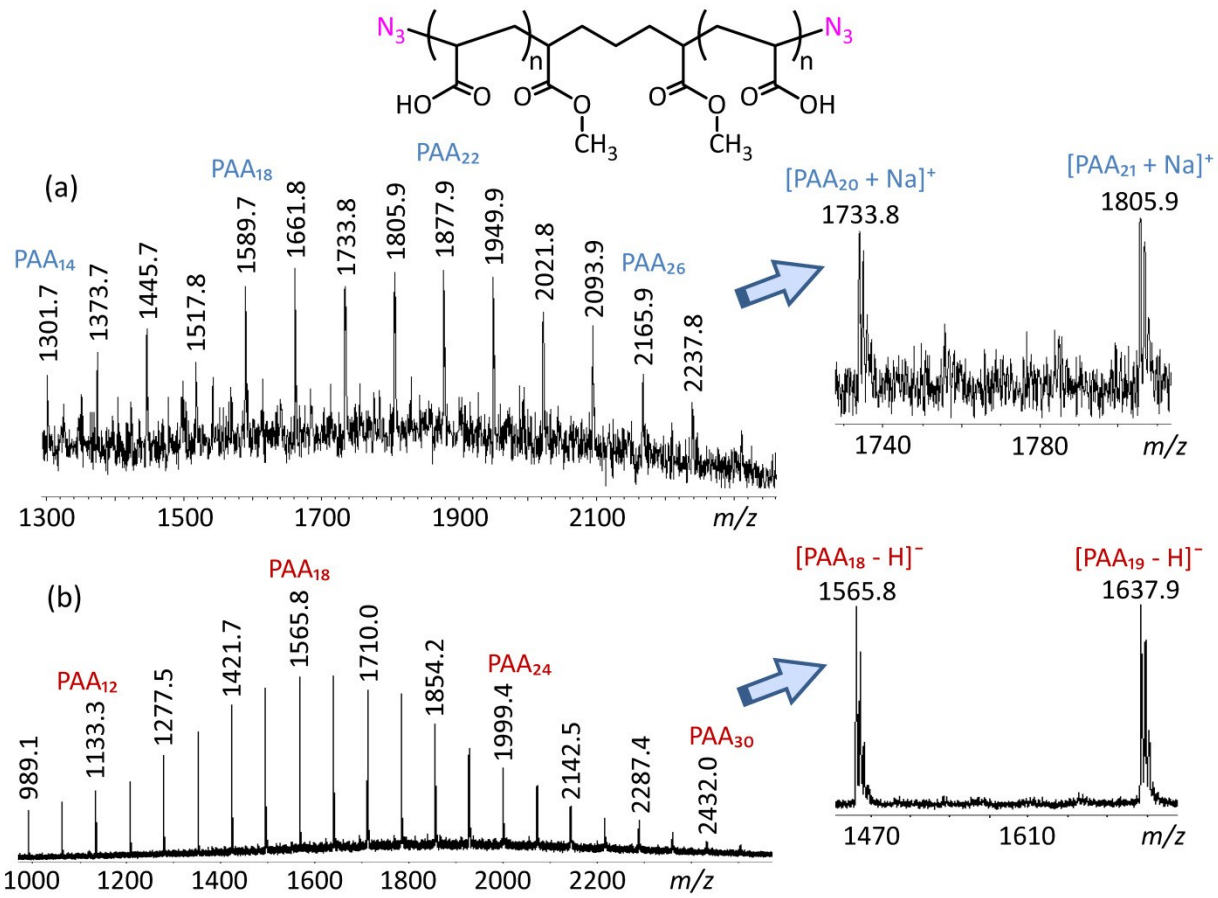

Fig. 4. MALDI mass spectra of telechelic poly(acrylic acid) diazide (PAA), acquired in (a) positive and (b) negative ion mode. The insets show expanded views.

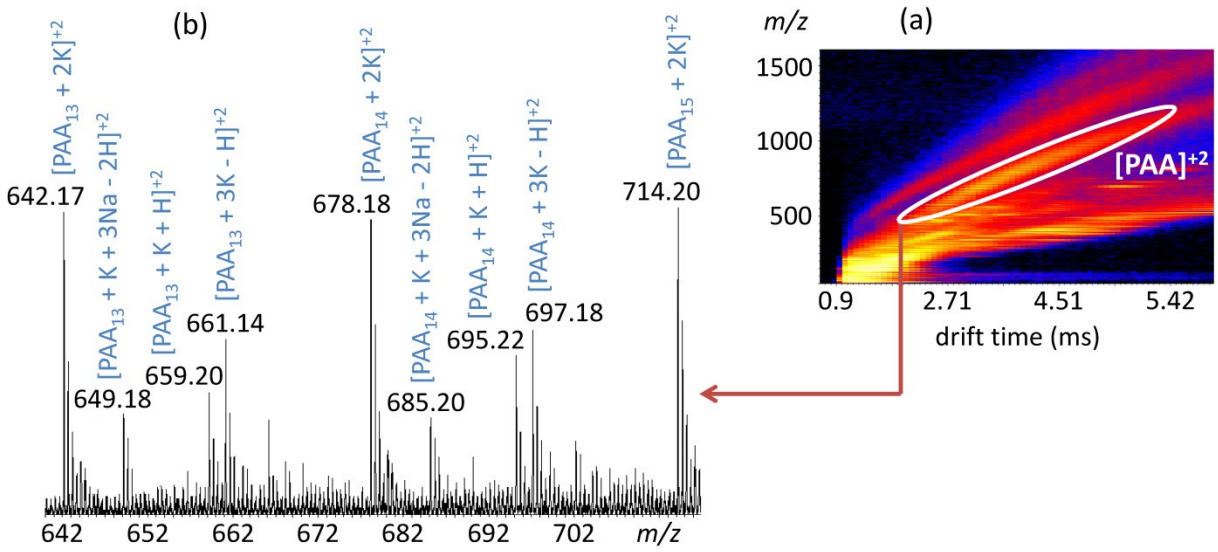

Fig. 5. (a) 2-D IM-MS plot (*m/z* vs. drift time) of diazide-terminated poly(acrylic acid), PAA, acquired in positive ion mode. The mobility region of doubly charged PAA is encased. (b) Mass spectrum extracted from the encased region, in which $[PAA + 2K]^{+2}$ cations dominate.

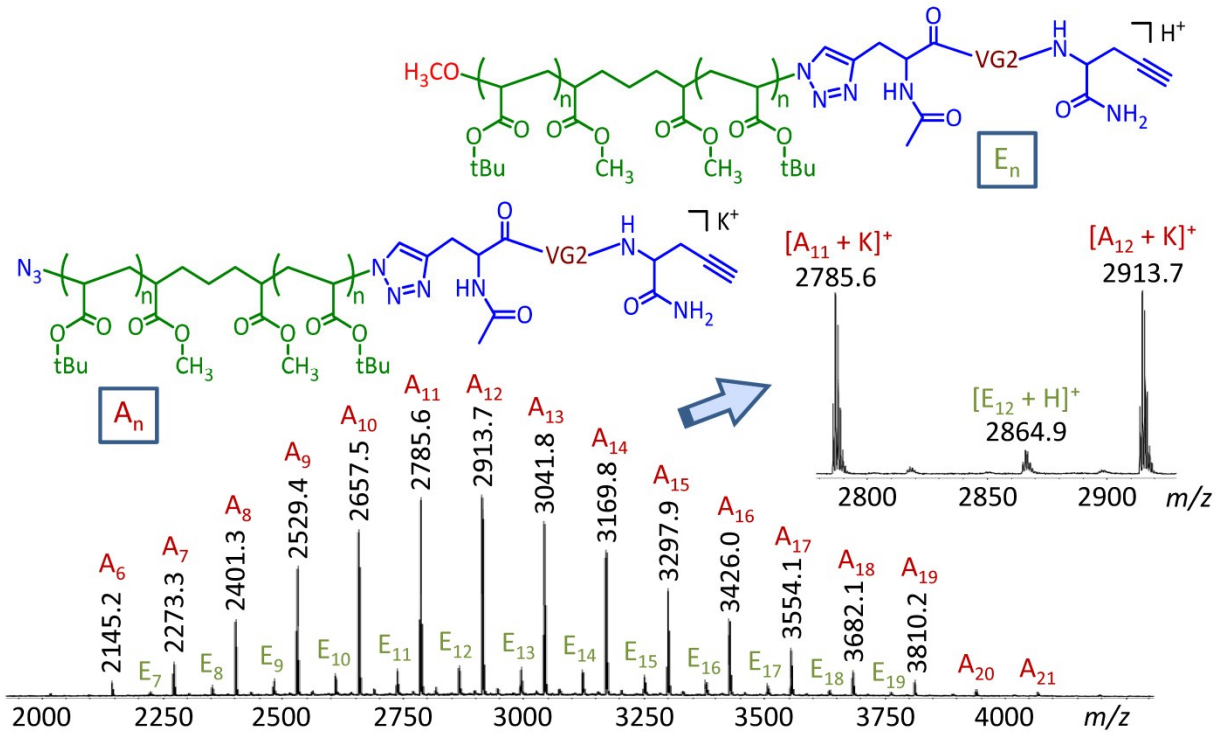

Fig. 6. MALDI mass spectrum of the P*t*BA–VG2 hybrid material in positive ion mode. The insets show an expanded view of the spectrum and the structures of the two major products detected.

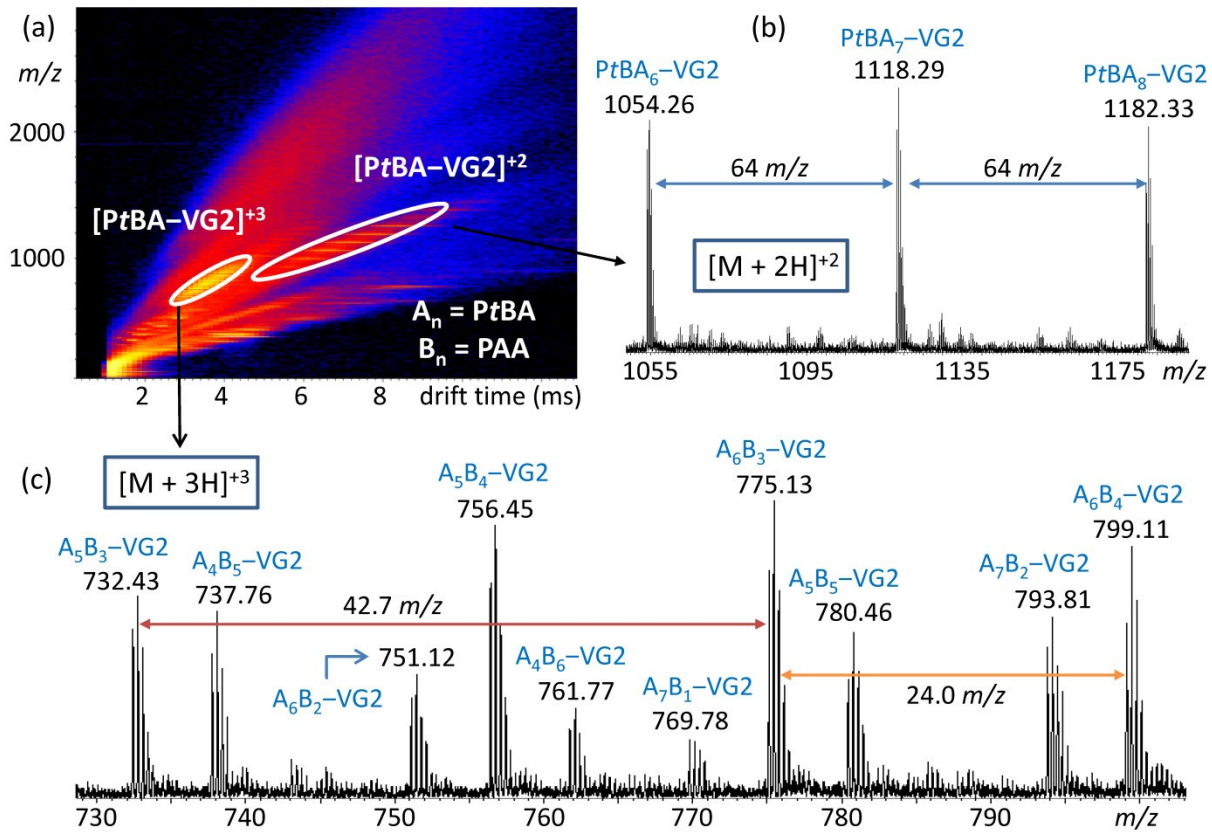

Fig. 7. (a) 2-D IM-MS plot of the P*t*BA–VG2 hybrid material in positive ion mode; the mobility regions of doubly and triply charged P*t*BA–VG2 cations are enclosed in ovals. (b,c) Mass spectra extracted from the mobility regions of (b) +2 and (c) +3 ions of P*t*BA–VG2, in which doubly and triply protonated oligomers, respectively, dominate. A and B designate P*t*BA and PAA repeat units, respectively.

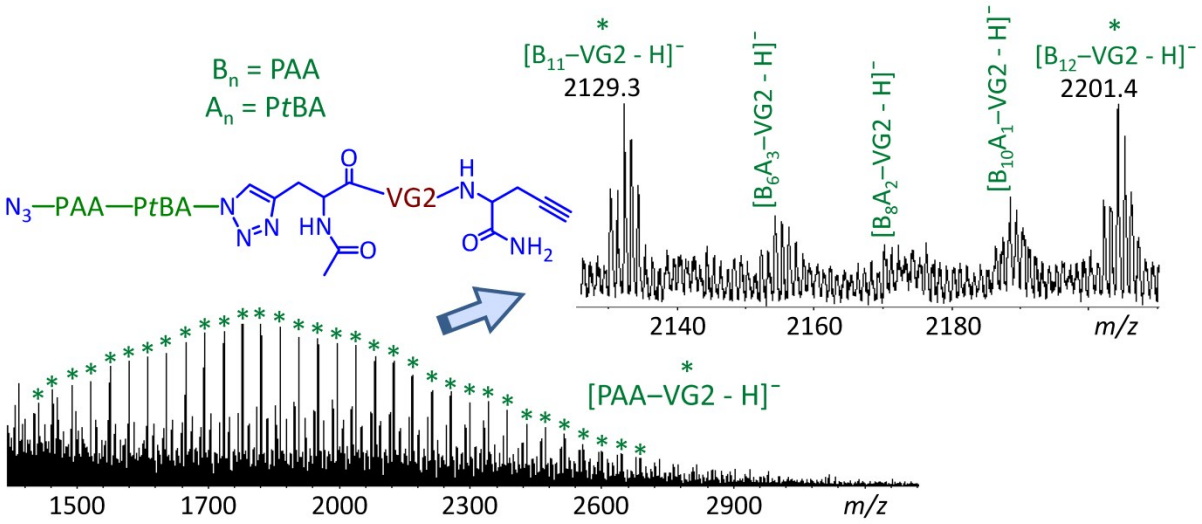

Fig. 8. MALDI mass spectrum of the PAA–VG2 hybrid material in negative ion mode; B_n and A_n designate the number of PAA and remaining (unhydrolyzed) P*t*BA repeat units, respectively. The main distribution (marked by *) arises from the completely hydrolyzed product.

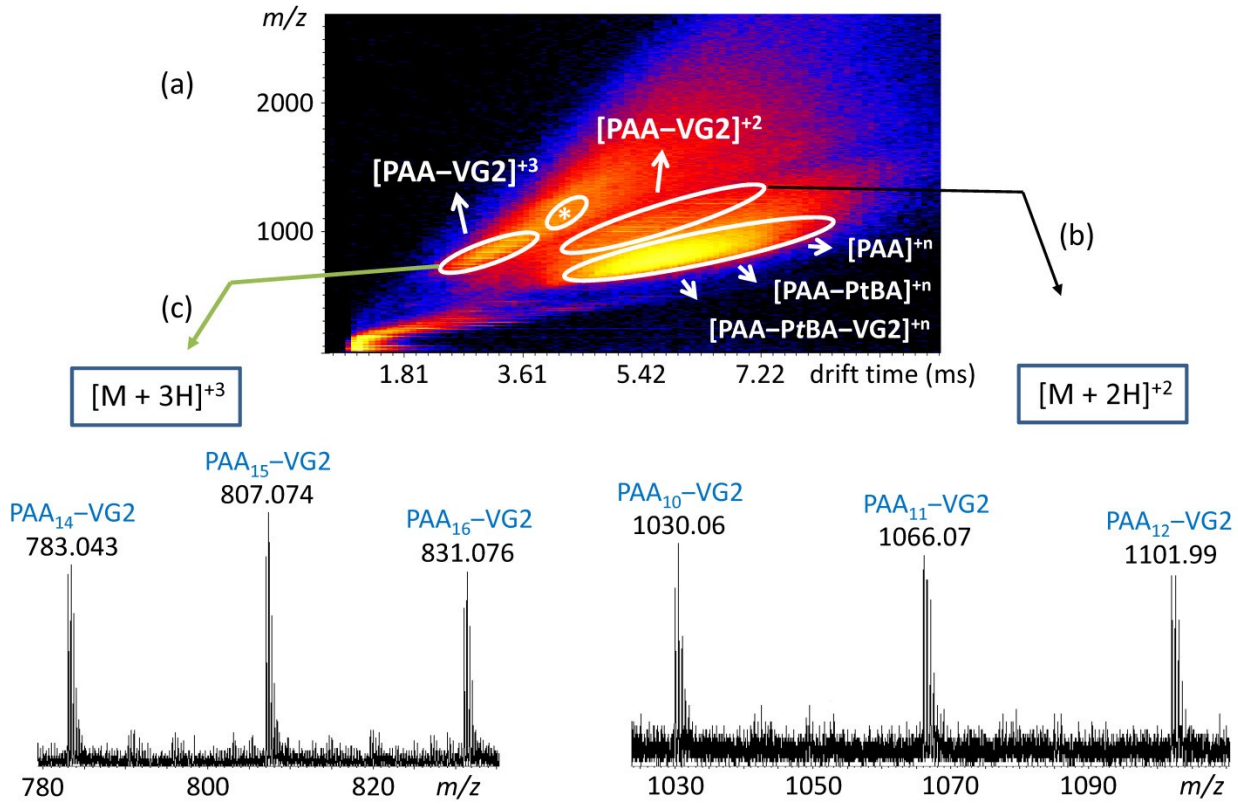

Fig. 9. (a) 2-D IM-MS plot of the PAA–VG2 hybrid material in positive ion mode; the mobility regions of doubly and triply charged PAA–VG2 cations and of incompletely hydrolyzed hybrid as well as unreacted polymer are enclosed in ovals. (b,c) Mass spectra extracted from the mobility regions of (b) +2 and (c) +3 ions of PAA–VG2, which contain doubly and triply protonated oligomers, respectively. The region marked with an asterisk contains +4 ions of $[PAA–VG2]_2$ oligomers (see text and Fig. 11a).

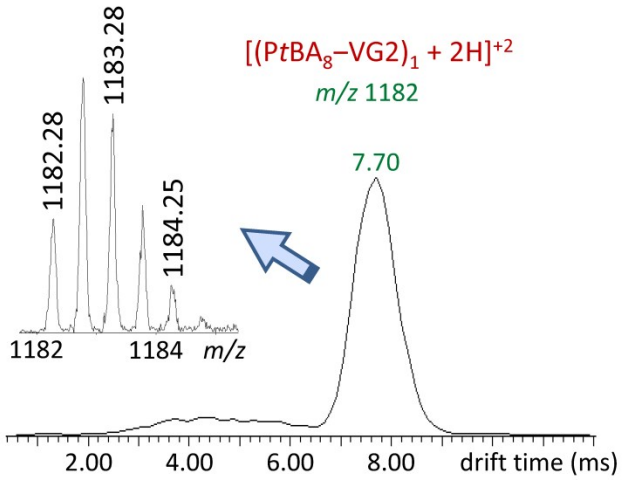

Fig. 10. IM-MS chromatogram of the ions at *m/z* 1182 from P*t*BA–VG2, showing the corresponding drift time distribution. The inset depicts the mass spectrum extracted from the main peak (centering at 7.70 ms).

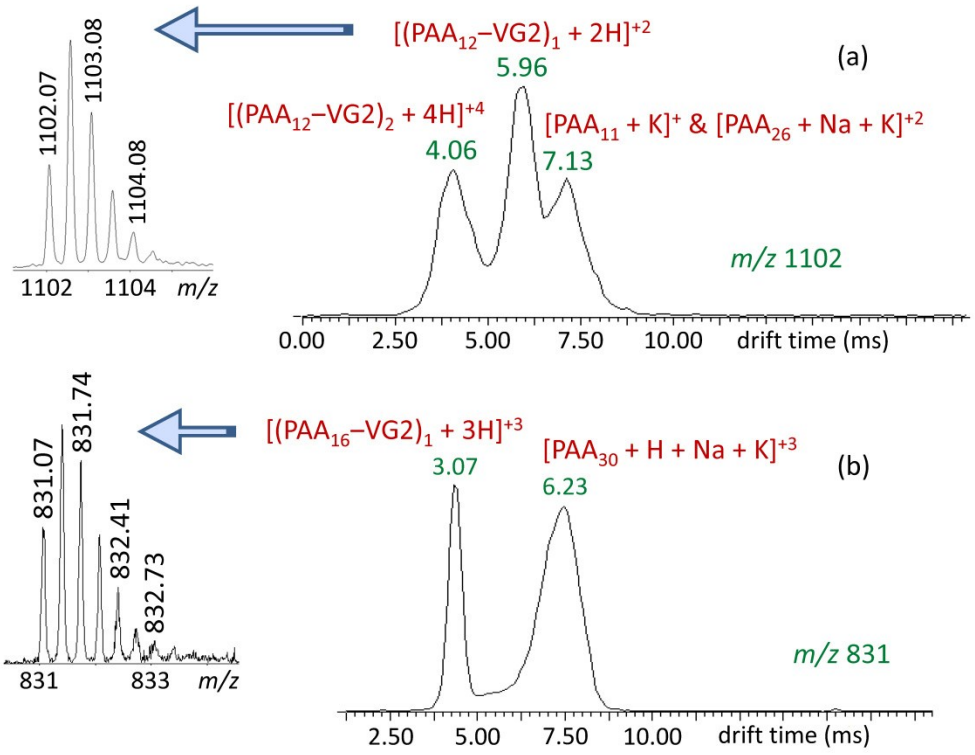

Fig. 11. IM-MS chromatograms of the ions at (a) *m/z* 1102 and (b) *m/z* 831from PAA–VG2, showing the corresponding drift time distributions. The insets depict the mass spectra extracted from the peaks centering at (a) 5.96 ms and (b) 3.07 ms.

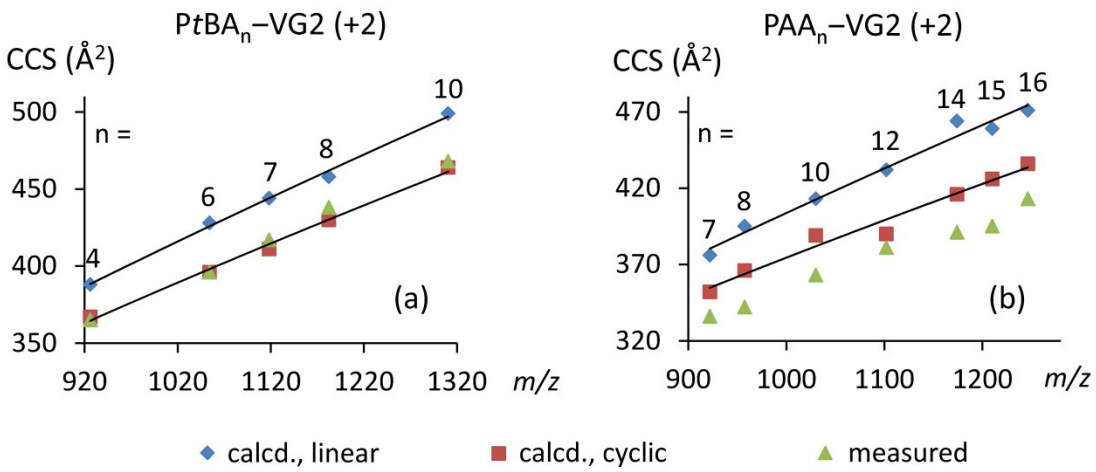

Fig. 12. Calculated collision cross-section (PA method) for doubly protonated oligomers of (a) P*t*BA–VG2 and (b) PAA–VG2 with linear or cyclic architecture, and experimental collision cross-section of the same ions vs. *m/z* ratio.